Research Article | Vol. 25, No. 14 | 10 Jul 2017 | OPTICS EXPRESS 15624
Optics EXPRESS

Zone plates as imaging analyzers for resonant inelastic x-ray scattering

FELIX MARSCHALL,* DANIEL MCNALLY, VITALIY A. GUZENKO, BENEDIKT RÖSNER, MARCUS DANTZ, XINGYE LU, LEONARD NUE, VLADIMIR STROCOV, THORSTEN SCHMITT, AND CHRISTIAN DAVID

Paul Scherrer Institut, CH-5232 Villigen PSI, Switzerland
**felix.marschall@psi.ch*

Abstract: We have implemented and successfully tested an off-axis transmission Fresnel zone plate as a novel type of analyzer optics for resonant inelastic x-ray scattering (RIXS). We achieved a spectral resolution of 64 meV at the nitrogen K-edge (E/dE = 6200), closely matching theoretical predictions. The fundamental advantage of transmission optics is the fact that it can provide stigmatic imaging properties. This opens up a variety of advanced RIXS configurations, such as efficient scanning RIXS, parallel detection for varying incident energy and time-resolved measurements.

OCIS codes: (050.1970) Diffractive optics; (110.4235) Nanolithography; (110.7440) X-ray imaging; (300.6330) Spectroscopy, inelastic scattering including Raman; (300.6560) Spectroscopy, x-ray; (340.7440) X-ray imaging.

References and links

1. S. Johnston, C. Monney, V. Bisogni, K.-J. Zhou, R. Kraus, G. Behr, V. N. Strocov, J. Málek, S.-L. Drechsler, J. Geck, T. Schmitt, and J. van den Brink, "Electron-lattice interactions strongly renormalize the charge-transfer energy in the spin-chain cuprate Li_2CuO_2," Nat. Commun. **7**, 10563 (2016).
2. V. Bisogni, S. Catalano, R. J. Green, M. Gibert, R. Scherwitzl, Y. Huang, V. N. Strocov, P. Zubko, S. Balandeh, J.-M. Triscone, G. Sawatzky, and T. Schmitt, "Ground-state oxygen holes and the metal-insulator transition in the negative charge-transfer rare-earth nickelates," Nat. Commun. **7**, 13017 (2016).
3. J. Schlappa, K. Wohlfeld, K. J. Zhou, M. Mourigal, M. W. Haverkort, V. N. Strocov, L. Hozoi, C. Monney, S. Nishimoto, S. Singh, A. Revcolevschi, J.-S. Caux, L. Patthey, H. M. Rønnow, J. van den Brink, and T. Schmitt, "Spin-orbital separation in the quasi-one-dimensional Mott insulator Sr2CuO3," Nature **485**(7396), 82–85 (2012).
4. K.-J. Zhou, M. Radovic, J. Schlappa, V. Strocov, R. Frison, J. Mesot, L. Patthey, and T. Schmitt, "Localized and delocalized Ti 3dcarriers in $LaAlO_3$/$SrTiO_3$superlattices revealed by resonant inelastic x-ray scattering," Phys. Rev. B **83**(20), 201402 (2011).
5. K.-J. Zhou, Y.-B. Huang, C. Monney, X. Dai, V. N. Strocov, N.-L. Wang, Z.-G. Chen, C. Zhang, P. Dai, L. Patthey, J. van den Brink, H. Ding, and T. Schmitt, "Persistent high-energy spin excitations in iron-pnictide superconductors," Nat. Commun. **4**, 1470 (2013).
6. J. Schlappa, T. Schmitt, F. Vernay, V. N. Strocov, V. Ilakovac, B. Thielemann, H. M. Rønnow, S. Vanishri, A. Piazzalunga, X. Wang, L. Braicovich, G. Ghiringhelli, C. Marin, J. Mesot, B. Delley, and L. Patthey, "Collective magnetic excitations in the spin ladder Sr14Cu24O41 measured using high-resolution resonant inelastic x-ray scattering," Phys. Rev. Lett. **103**(4), 047401 (2009).
7. M. P. M. Dean, R. S. Springell, C. Monney, K. J. Zhou, J. Pereiro, I. Božović, B. Dalla Piazza, H. M. Rønnow, E. Morenzoni, J. van den Brink, T. Schmitt, and J. P. Hill, "Spin excitations in a single La2CuO4 layer," Nat. Mater. **11**(10), 850–854 (2012).
8. M. P. M. Dean, Y. Cao, X. Liu, S. Wall, D. Zhu, R. Mankowsky, V. Thampy, X. M. Chen, J. G. Vale, D. Casa, J. Kim, A. H. Said, P. Juhas, R. Alonso-Mori, J. M. Glownia, A. Robert, J. Robinson, M. Sikorski, S. Song, M. Kozina, H. Lemke, L. Patthey, S. Owada, T. Katayama, M. Yabashi, Y. Tanaka, T. Togashi, J. Liu, C. Rayan Serrao, B. J. Kim, L. Huber, C. L. Chang, D. F. McMorrow, M. Först, and J. P. Hill, "Ultrafast energy- and momentum-resolved dynamics of magnetic correlations in the photo-doped Mott insulator Sr2IrO4," Nat. Mater. **15**(6), 601–605 (2016).
9. G. Ghiringhelli, A. Piazzalunga, C. Dallera, G. Trezzi, L. Braicovich, T. Schmitt, V. N. Strocov, R. Betemps, L. Patthey, X. Wang, and M. Grioni, "SAXES, a high resolution spectrometer for resonant x-ray emission in the 400-1600eV energy range," Rev. Sci. Instrum. **77**(11), 113108 (2006).
10. J. Nordgren, G. Bray, S. Cramm, R. Nyholm, J.-E. Rubensson, and N. Wassdahl, "Soft x-ray emission spectroscopy using monochromatized synchrotron radiation (invited)," Rev. Sci. Instrum. **60**(7), 1690–1696 (1989).

#287666 https://doi.org/10.1364/OE.25.015624
Journal © 2017 Received 28 Feb 2017; revised 26 May 2017; accepted 18 Jun 2017; published 26 Jun 2017

Optics EXPRESS

11. V. N. Strocov, T. Schmitt, U. Flechsig, L. Patthey, and G. S. Chiuzbăian, "Numerical optimization of spherical variable-line-spacing grating X-ray spectrometers," J. Synchrotron Radiat. **18**(2), 134–142 (2011).
12. V. N. Strocov, T. Schmitt, U. Flechsig, T. Schmidt, A. Imhof, Q. Chen, J. Raabe, R. Betemps, D. Zimoch, J. Krempasky, X. Wang, M. Grioni, A. Piazzalunga, and L. Patthey, "High-resolution soft X-ray beamline ADRESS at the Swiss Light Source for resonant inelastic X-ray scattering and angle-resolved photoelectron spectroscopies," J. Synchrotron Radiat. **17**(5), 631–643 (2010).
13. T. Warwick, Y.-D. Chuang, D. L. Voronov, and H. A. Padmore, "A multiplexed high-resolution imaging spectrometer for resonant inelastic soft X-ray scattering spectroscopy," J. Synchrotron Radiat. **21**(4), 736–743 (2014).
14. V. N. Strocov, "Concept of a spectrometer for resonant inelastic X-ray scattering with parallel detection in incoming and outgoing photon energies," J. Synchrotron Radiat. **17**(1), 103–106 (2010).
15. J. Rehanek, F. Schäfers, H. Löchel, A. Firsov, J. Grünert, W. Freund, C. Ozkan, S. Molodtsov, and A. Erko, "A case study of novel X-ray Optics for FEL sources," J. Phys. Conf. Ser. **425**(5), 052013 (2013).
16. E. Abbe, „Die Lehre von der Bildentstehung im Mikroskop", page 10, Braunschweig, Vieweg, 1910.
17. H. Wolter, "Spiegelsysteme streifenden Einfalls als abbildende Optiken für Röntgenstrahlen," Ann. Phys. **10**(1), 94–114 (1952).
18. J. L. Soret, "Ueber die durch Kreisgitter erzeugten Diffractionsphänomene," Annalen der Physik und Chemie **232**(9), 99–113 (1875).
19. B. L. Henke, E. M. Gullikson, and J. C. Davis, "X-Ray Interactions: Photoabsorption, Scattering, Transmission, and Reflection at E = 50-30,000 eV, Z = 1-92," At. Data Nucl. Data Tables **54**(2), 181–342 (1993).
20. S. Matthew, "High-resolution detectors for soft X-ray spectroscopy," PhD thesis, The Open University (2014).
21. T. Schmitt, V. N. Strocov, K.-J. Zhou, J. Schlappa, C. Monney, U. Flechsig, and L. Patthey, "High-resolution resonant inelastic X-ray scattering with soft X-rays at the ADRESS beamline of the Swiss light source: Instrumental developments and scientific highlights," J. Electron Spectrosc. Relat. Phenom. **188**, 38–46 (2013).
22. J. Vila-Comamala, K. Jefimovs, J. Raabe, T. Pilvi, R. H. Fink, M. Senoner, A. Maassdorf, M. Ritala, and C. David, "Advanced thin film technology for ultrahigh resolution X-ray microscopy," Ultramicroscopy **109**(11), 1360–1364 (2009).
23. G. Schneider, "Zone plates with high efficiency in high orders of diffraction described by dynamical theory," Appl. Phys. Lett. **71**(16), 2242–2244 (1997).
24. V. A. Guzenko, J. Romijn, J. Vila-Comamala, S. Gorelick, C. David, I. McNulty, C. Eyberger, and B. Lai, "Efficient E-Beam Lithography Exposure Strategies for Diffractive X-ray Optics," AIP Conf. Proc. **1365**, 92–95 (2011).

1. Introduction

High-resolution RIXS in the ultraviolet and soft X-ray range is particularly sensitive to the electronic properties of matter owing to its strong coupling to valence electrons. This allows for detailed studies of strongly correlated electron systems such as transition metals and rare earth oxides. RIXS is a powerful probe of excitations from the electronic ground state of such correlated materials involving lattice [1], charge [2], orbital [3,4] and spin [5–7] degrees of freedom. With extremely high spectral resolution one can employ the scattering and incident angle dependence of the RIXS signal for analyzing the collective behavior of charge, orbital and spin excitations by assessing their momentum dependence. Moreover, RIXS also has interesting applications for a wider range of molecular samples, including gases and liquids. It for instance probes the detailed bonding environment in metallo-organic complexes and the charge transfer process in electrochemical active materials like the cathodes in batteries. Combined with pump-probe techniques, the ultra-fast dynamics of a sample become accessible when implementing RIXS experiments at X-ray free-electron laser (XFEL) sources [8].

Typically, spectrometers based on spherical reflection gratings with varying line spacing (VLS) [9] or constant line density (Rowland type spectrometers) [10] are used to collect the radiation emitted from the sample and to disperse it across a CCD detector [see Fig. 1(a)]. The gratings are fabricated on spherical surfaces that provide focusing in the energy dispersive direction. However, the focusing in the sagittal direction is only weak, and the dispersed signal is spread out along the non-dispersive direction of the detector. Therefore, in RIXS set-ups using VLS gratings on spherical surfaces, the detector signal is integrated (projected) along the non-dispersive direction, that conveys no information about the sample [11,12].

Optics EXPRESS

Recent concepts [13,14] aim at exploiting the non-dispersive direction on a RIXS detector to obtain additional information. It has been suggested to illuminate the sample with a line focus in the non-dispersive direction, in which the energy of the incident photons is varied. With this approach, one could simultaneously measure RIXS spectra over a range of incident energies – a technique referred to as hv^2 spectrometry [14,15]. Further ideas are to use a monochromatic line focus for acquiring spatially resolved RIXS spectra, or for time resolved experiments.

The key problem of this approach is that a single bounce reflecting optics will not provide aberration free imaging conditions (stigmatic imaging), resulting in a severe loss of spatial and spectral resolution. In order to maintain acceptable imaging properties, that fulfil the Abbe sine condition [16], two elliptical reflecting optics arranged in a Wolter-type I arrangement need to be used in series [13,17]. This greatly increases the cost and complexity of the detection system, decreases throughput, and makes alignment a true challenge.

To overcome these issues, we used an off-axis transmission Fresnel zone plate (FZP) as analyzer, as shown in Fig. 1(b). Transmission FZPs are frequently used in x-ray imaging applications and are known to provide stigmatic imaging properties [18]. They are very insensitive to angular alignment and stability, which greatly facilitates their use compared to reflective optical elements. However, so far they have seldom been considered as optics in analyzer geometries. The essential mathematical relations for the design of an off-axis transmission FZP to be used as analyzer in emission spectroscopy, and its performance in terms of spectral resolution are derived below.

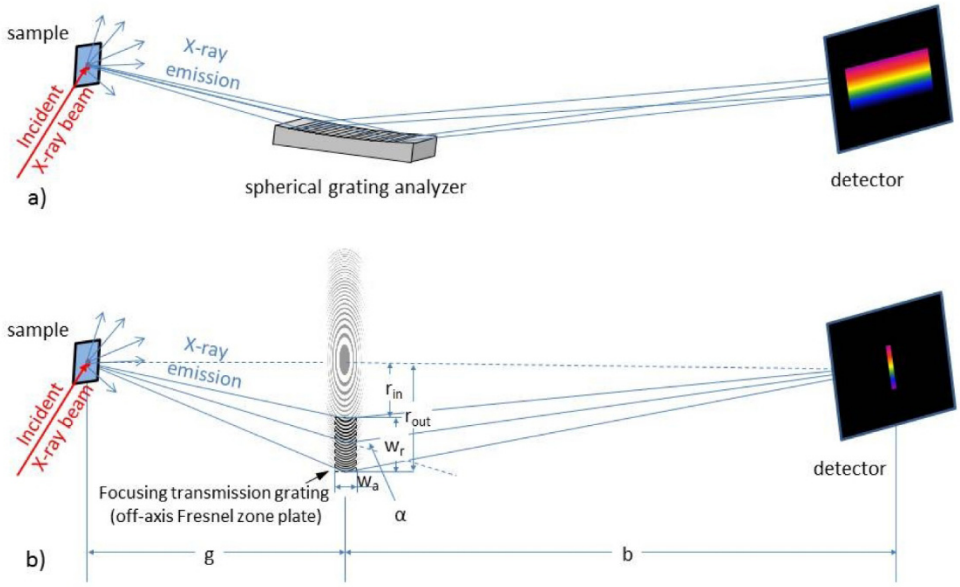

Fig. 1. a) Schematic view of a conventional RIXS detection scheme using a reflective grating. b) Proposed detection scheme using an off-axis transmission FZP. The grating can be seen as the off-axis part of the FZP indicated in grey.

2. Theoretical description

We first consider the case illustrated in Fig. 1(b) and radiation at a design energy E_0, corresponding to a wavelength $\lambda_0 = hc/E_0$. We intend to image the source point, i.e., the part of the sample that is illuminated with x-rays having a wavelength of λ_0 onto a detector. The straight line from source point to the detector, see dashed line in Fig. 1(b), defines the optical axis of our setup. The FZP used for imaging consists of concentric rings around this axis.

Optics EXPRESS

From zone to zone the optical path length must increase by λ/2, which leads to the geometric relation:

$$\sqrt{g^2+r_n^2}+\sqrt{b^2+r_n^2}=g+b+\frac{n\lambda}{2} \tag{1}$$

with the distance g between the sample and the FZP center and the distance b between the FZP center and the detector and the radius r_n of the n^{th} zone. Solving (1) for r_n^2, the zone radii must fulfil the equation:

$$r_n^2=\frac{gb(g+b)n\lambda+\frac{1}{4}\left[(g+b)^2+gb\right](n\lambda)^2+\frac{1}{8}(g+b)n\lambda^3+\frac{1}{64}(n\lambda)^4}{\left(g+b+n\frac{\lambda}{2}\right)^2} \tag{2}$$

where an odd number for n describes the inner radius of a ring and an even number the outer radius.

According to the lens maker's equation, we can attribute a focal length f to such a FZP:

$$f=\frac{gb}{g+b} \tag{3}$$

and allocate a magnification factor $m = b/g$.

In our case, we do not use a full FZP, but only an off-axis part consisting of arcs, as illustrated in Fig. 1(b). In the radial direction this part extends over the width w_r from an inner radius r_{in} to an outer radius r_{out}, with the corresponding zone numbers n_{in} and n_{out}. The width in the azimuthal direction is denominated as w_a.

The focal length of a FZP defined in (3) is often approximated by the well know relation, $f \approx r_n^2/n\lambda \approx r_n^2/nhc$ and therefore in a good approximation proportional to the photon energy. Radiation with different wavelengths will produce image points on the optical axis at different distances from the FZP plane. For a fixed detector distance b_0 any radiation with energies deviating from E_0 will be defocused. Simple geometric considerations show, that for an energy deviation of ΔE, the corresponding distance between the focused plane and the detector plane at b_0 is in good approximation given by:

$$\Delta b \approx (m+1)^2\,\Delta f \approx (m+1)^2\,\frac{\Delta E r_n^2}{nhc} \tag{4}$$

and the corresponding change in spot size on the detector caused by the zone plate's chromaticity is:

$$\Delta x \approx \left|\Delta b\frac{w_r}{b}\right| \approx \left|w_r\,(m+1)^2\,\frac{\Delta E r_n^2}{nhcb}\right| \tag{5}$$

In order to derive the basic optical properties of an off-axis FZP used as analyzer at its design energy E_0, we consider for now only incremental changes in energy so we can neglect chromatic effects. Moreover, we assume, that w_r is small compared to $r_{\min}$, and that the wavelength is small compared to the zone widths dr_n. If we now consider an x-ray passing through the off-axis FZP at the radius r_n, it will be diffracted by the angle $a_n \approx \lambda/dr_n \approx hc/(E \times dr_n)$, where $dr_n = r_n - r_{n-1}$ is the width of the n^{th} zone. The angular dispersion is therefore given by:

$$\frac{d\alpha_n}{dE}=\frac{hc}{2dr_n}\frac{1}{E^2} \tag{6}$$

Optics EXPRESS

and the dispersion in the detector plane is:

$$\frac{dx_n}{dE} \approx \frac{hc}{2dr_n}\frac{b}{E^2} \tag{7}$$

The energy resolution of a spectrometer based on an off-axis FZP is determined by three contributions. (i) Assuming a spatial resolution that is given by 2.5 × oversampling and a pixel size p, we can derive the detector-limited contribution of

$$dE_{det} \approx 2.5p\frac{2dr_n}{hc}\frac{E^2}{b} \tag{8}$$

(ii) Assuming monochromatic radiation, the size s of the spot on the sample will be magnified onto the detector by the imaging ratio b/g. This results in a geometric contribution to the energy resolution of

$$dE_{geo} \approx s\frac{b}{g}\frac{2dr_n}{hc}\frac{E^2}{b} \approx s\frac{2dr_n}{hc}\frac{E^2}{g} \tag{9}$$

(iii) The radial aperture size w_r of the off-axis FZP gives a diffraction limited contribution to the spot size on the detector. This effect limits the resolving power $E/\mathrm{d}E$ to the number of zones $n_{\mathrm{out}} - n_{\mathrm{in}}$ inside the off-axis FZP. As we assume the width of the FZP to be small compared to its full radius, the zone width only varies slightly over the off-axis FZP. Thus, we assume a constant period inside the off-axis FZP for the calculations. We can therefore approximate the diffraction-limited contribution by

$$dE_{diff} \approx \frac{E}{n_{out} - n_{in}} \approx E\frac{2dr_n}{w_r} \tag{10}$$

The energy resolution of the spectrometer is then limited to the geometrical mean of all three contributions:

$$dE_{spec} \approx \sqrt{dE_{det}{}^2 + E_{geo}{}^2 + E_{diff}{}^2} \tag{11}$$

As all three contributions to this term depend on the zone width dr_n, it is essential to produce off-axis FZPs with narrow structures. Moreover, it is evident that the resolution is best for low photon energies. Figure 2 shows the calculated resolving power for some relevant

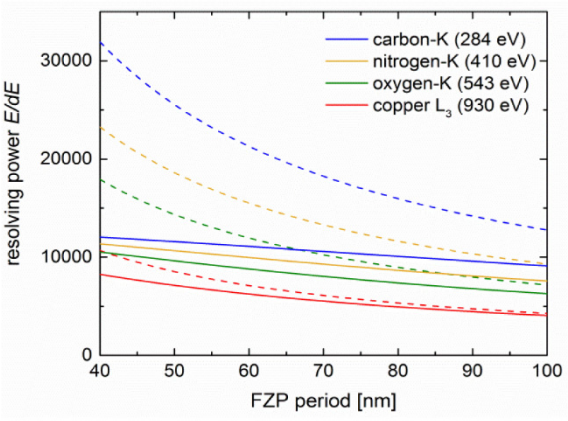

Fig. 2. Calculated resolving power E/dE_{spec} of the RIXS spectrometer (dashed lines) and total resolving power E/dE_{tot} taking into account the incident bandwidth (solid line) vs. FZP period $2dr_n$ for photon energies at a selection of relevant absorption edges. The spot size on the sample is s = 5 µm (with 10 µm monochromator exit slits), sample distance g = 1.75 m, detector distance b = 2.9 m, grating size w = 3 mm, effective subpixel size sp = 1.37 µm of the

Optics EXPRESS

tilted detector, 2.5 × oversampling, incoming bandwidth E/dE_{BW} = 13000 (using a monochromator grating with 800 lines/mm).

absorption edges under the constraints given by the RIXS spectrometer geometry at the ADRESS beam line of the Swiss Light Source (SLS) [12], also taking into account the contribution of the incoming bandwidth $E/dE_{BW} = 13000$.

$$dE_{tot} \approx \sqrt{dE_{det}^{\ 2} + E_{geo}^{\ 2} + E_{diff}^{\ 2} + E_{bw}^{\ 2}} \tag{12}$$

3. Experimental Setup

Our experiments were carried out at the ADRESS beamline at the Swiss Light Source (SLS) [12]. The ADRESS beamline is ideally suited for the experiment. It provides the intense, narrow-band beam (10^{13} photons/sec within 0.01% bandwidth at 1 keV photon energy) required to assess the performance of our analyzer inserted in the current spectrometer arm at the ADRESS beamline. Furthermore, it features a high-resolution, spherical VLS analyzer and detector system serving as benchmark for our FZP analyzer optics. The reflective high resolution grating available at the ADRESS-RIXS spectrometer has a central groove density of 3000 lines/mm with variable line spacing (2945 lines/mm to 3055 lines/mm) optimized to deliver the required focal distance and slope of the focal curve at the CCD detector [11,21]. The last upgrade of the optics and CCD detector of the spectrometer has pushed its resolving power to better than 20000 at 1 keV photon energy.

For our demonstrator experiments, we chose the photon energy range around 397 eV, as it coincides with the scientifically relevant resonant excitation of nitrogen. The beam from the monochromator was focused onto the sample with an ellipsoidal refocusing mirror working at a demagnification of 5.85, which delivers a beam of 3.9 µm × 54 µm (v × h), resulting in a footprint on the sample of 3.9 µm × 76 µm (v × h) for 45° incidence angle. In our case the monochromator exit slits were only closed to 10 µm, resulting in a vertical spot size on the sample of about 5 µm. Our optic was mounted on a manual UHV manipulator allowing us to insert and position it into the ADRESS-RIXS analyser arm at about g = 1.75 m from the sample. The detector was placed b = 2.9 m behind the optic, resulting in a magnification of $m = b/g$ = 1.66. For the design of the optic an area of 3 mm × 3 mm was taken from the outermost edge of a FZP with diameter of 98.64 mm and 70 nm outermost period, resulting in a focal length of 1.09 m at 397 eV and an average deflection angle of α = 2.5°. The simple manual UHV manipulator with the optic just mounted on the end of a rod was sufficient as transmission FZPs are very insensitive to angular alignment errors and no angular adjustment is required. As the FZP pattern was defined by a very accurate lithography process (see below) the focal length for a given photon energy is precisely known. Moreover, the depth of focus of our spectrometer setup is several millimeters, therefore the positioning along the optical axis does not need to be precise.

The optic was fabricated from negative photo resist HSQ (Hydrogen silsesquioxane). Therefore a square shaped silicon nitride membrane with 3 mm × 3 mm size and 100 nm thickness was spin coated with 400 nm HSQ. The HSQ was structured by 100 kV electron beam lithography using a Raith/Vistec EBPG 5000PlusES system. With a dose of 10000 µC/cm^2 and a beam current of 5 nA, the exposure of the 41537 zones of a lens with 70 nm outermost period took around 50 h. Due to exposure HSQ becomes similar to SiO_2, which is non-soluble in the Microposit AZ351 developer used for removing the non-exposed regions. Figure 3 shows SEM micrographs of the edge of a FZP.

Optics EXPRESS

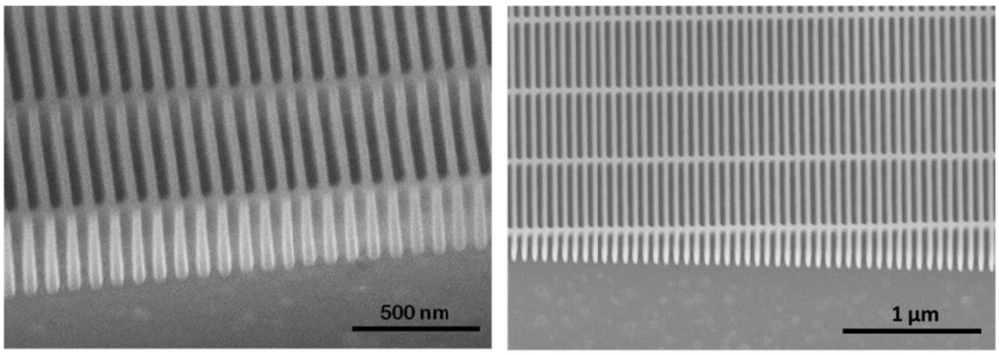

Fig. 3. SEM micrographs of the edge of off-axis transmission FZPs made from HSQ (left) top view with 70 nm period (right) and viewed under 45° with 80 nm pitch. In both cases the structures are 400 nm high.

The theoretical efficiency of a diffraction grating with 70 nm pitch and 400 nm height made from HSQ is about 19% at 397 eV [19]. The transmission of the silicon nitride membrane with 100 nm thickness is about 68%, resulting in an overall theoretical efficiency of the optics of about 13%. Experience shows that the real efficiency of optics with such small zone widths is about half of the theoretical value, due to deviations of the real zone profile compared to the ideal shape. The size of the optics with 3 mm × 3 mm at a distance of 1.75 m from the sample results in a solid angle of collection of roughly 2.9×10^{-6} sr. The corresponding solid angle for the ADRESS-RIXS spectrometer with the gratings at ~1 m from the sample and 3 × CCD cluster detector in ~5 m from the sample, is 1.7×10^{-4} and the real grating efficiency is about 2 and 6% for the two gratings with resolving powers of about 27000 and 18000 at 400 eV, respectively. Although the solid angle of the FZP spectrometer still remains smaller compared to that of the grating, it can be increased in future, by increasing the FZP size, by clustering several FZPs, and by decreasing the distance from the sample.

The detector system RIXSCam from XCAM Ltd. consisted of three horizontally arranged CCD-chips with 1608 × 1632 pixels each. The pixel size was 16 µm × 16 µm. The detector was tilted 20° with respect to the optical axis, resulting in an effective pixel size of 5.47 µm in the energy dispersive direction. Furthermore, the detector provides subpixel resolution by interpolating from charge sharing utilizing a single photon counting algorithm [20] which further reduces resolution of the untilted detector below 4 µm. Taking into account the tilting of the detector, effective subpixel size is about 1.37 µm. This value is taken for the calculations.

In order to test the resolution performance of our optics, we recorded the elastic peak after scattering the incident x-rays on a carbon tape allowing a high yield for elastic scattering. The spectrum was recorded near specular and with vertical incident polarization to maximize the elastic scattering.

4. Results

After the alignment of the setup, a clear but weak signal was recorded on the detector [see Fig. 4]. In contrast to the original setup using a reflective grating, where the elastic peak forms a line on the detector, our stigmatic imaging optics produced a small circular spot, which is actually the magnified image of the illuminating beam on the sample.

Optics EXPRESS

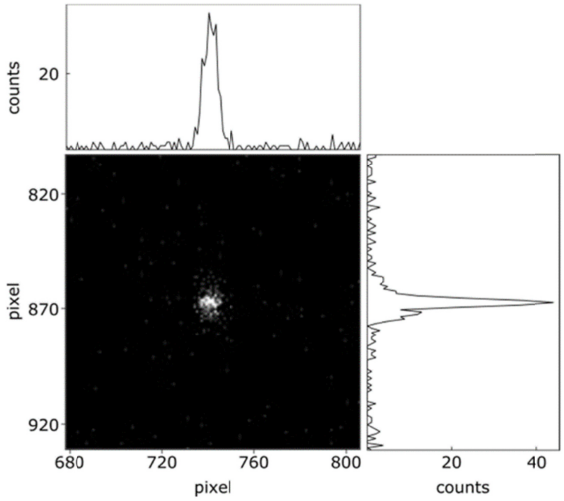

Fig. 4. Focal spot on the CCD detector, recorded at 397 eV, 10 µm monochromator exit slit, and 20 min exposure time. In the energy dispersive (vertical) direction, the FWHM of the spot was 4 pixel (21.8 µm). In the horizontal direction the FWHM was 10 pixel (160 µm). Both match the theoretical calculations concerning a real spot size of around 5 µm provided by the refocusing system [12], taking into account mechanical drift of 4 µm due to the long exposure time, a magnification of 1.7 and the chromatic broadening of 13 µm as result of the incoming bandwidth.

We performed an energy scan to confirm that the best focusing was achieved at the design energy of E_0 = 397 eV, see Fig. 5. The scan shows how the spectral resolution degrades when moving away from the design energy, a reasonable resolution can be maintained only over energy band of a few eV. The theoretical prediction for the chromatic aberration according to Eq. (5) are in reasonable agreement, the slope corresponds well with the trend of the measured data for larger deviations from the design energy.

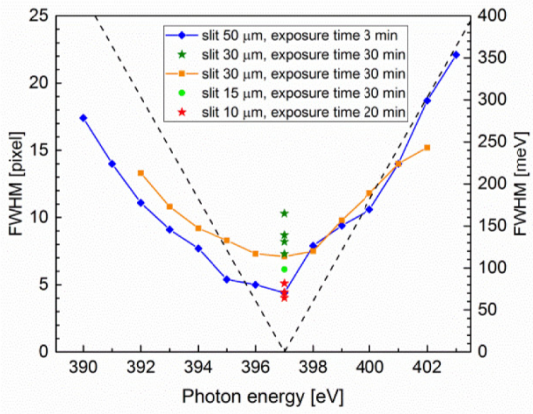

Fig. 5. Measured vertical FWHM of the spot on the CCD in the energy dispersive direction, dependent on photon energy. The smallest FWHM of 4 pixel (21.8 µm), was achieved at the design energy E_0 = 397 eV with the 10 µm monochromator exit slits. The dashed lines show the predicted chromaticity according to Eq. (5).

Additionally, we found that the focal spot size was dependent on conditions of the refocusing system providing the illumination of the sample. A bigger illuminated spot resulted in a bigger spot on the detector, as the used off-axis FZP provides stigmatic imaging conditions. Consequently the smallest spot size was achieved by closing down the

Optics EXPRESS

monochromator exit slits to 10 µm. Furthermore, the spot size was affected by the exposure time. Scans with shorter exposure time showed smaller spot sizes than scans with longer exposure time, which most likely is caused by mechanical and thermal drift. This is obvious when comparing to the scan with 50 µm monochromator exit slits and 3 min exposure time. The result of this measurement is nearly as good as the one with 10 µm monochromator exit slits and 20 min exposure time. 10 µm monochromator exit slits result in a spot size on the sample of 5 µm, whereas 50 µm exit slits result in spot size of 9.6 µm. Taking into account the slightly better result of the 10 µm measurement, the overall drift in the experimental setup was 4 µm in 20 min, including all drifts from storage ring, beamline, sample, optics holder, detector etc.. The causes of these drifts are slight temperature changes in the experimental hall of the Swiss Light Source, and a separate enclosure would be required to improve stability.

When changing the photon energy, the spot on the detector moved in the vertical direction due to the dispersion of the off-axis transmission FZP. The focal spot on the detector moved 62 pixels (339 µm) per eV [see Fig. 6]. For the smallest achieved spot size the FWHM was 4 pixels (21.8 µm) in the energy dispersive direction. This results in an energy resolution of 64 meV at 400 eV (resolving power E/dE = 6200).

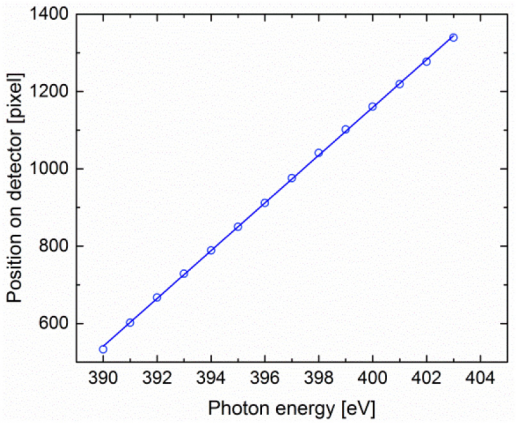

Fig. 6. Measured vertical spot position on CCD versus incident photon energy. The position of the focal spot was shifted by 62 pixels (339 µm) per eV. The size of the spot changed according to the imaging equation as the system was focused for 397 eV as shown in Fig. 5. The line represents the predicted dispersion according to Eq. (5).

This result is in very good agreement with the calculations. With the assumptions made for Fig. 2 and an effective spot size of 9 µm on the sample (including 4 µm drift), the calculated energy dispersion is 339 µm/eV (see Eq. (7)). For the energy resolving power, the contribution of the detector to the limit of the resolving power is dE_{det}/E = 37828 (see Eq. (8)), the geometric contribution is dE_{geo}/E = 8675 (see Eq. (9)), the diffraction contribution is dE_{diff}/E = 42857 (see Eq. (10)) and the contribution of the incoming bandwidth is dE_{BW}/E = 13000, which leads to a total resolving power of dE_{tot}/E = 6993 (see Eq. (12)). Clearly the geometric term is the most significant contribution to the energy resolution of the spectrometer. Consequently, a reduction of the spot size on the sample and the drift will significantly improve the resolution of the setup. Additionally, the incoming bandwidth has to be reduced for higher resolutions by changing to a finer monochromator grating [12].

Optics EXPRESS

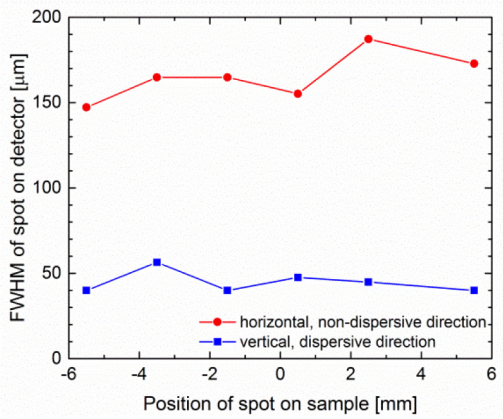

Fig. 7. FWHM of focus at 397 eV photon energy for varying horizontal position of the incident beam on the sample. The resulting resolution remains constant, the small changes of the FWHM are due to the low signal-to-noise ratio. The different size in horizontal and vertical direction is a result of the shape of the spot on the sample. According to this measurement with a monochromator exit slit size of 30 µm and 30 min exposure time the spot size on the CCD was about 160 µm × 50 µm.

The major advantage of our setup is the stigmatic imaging condition provided by the transmission FZP. The observation of a finite horizontal spot size is a clear proof of imaging in the horizontal direction. With the reflective grating typically used for RIXS experiments the signal is spread horizontally over the entire detector. To confirm the imaging quality of our configuration, we moved the illumination spot horizontally across the sample, without observing any significant change in the shape or size of the focal spot [see Fig. 7]. The position of the spot on the detector remained constant in the energy dispersive direction and moved horizontally according to the movement of the illuminating spot. No off-axis aberrations could be detected for our FZP analyzer optics.

The spot on the CCD was not circular, but horizontally three times bigger than vertically (h × v = 160 µm × 50 µm), which is in good agreement with the description of the beamline by Strocov et al. [12], taking into account the not fully closed (30 µm) monochromator exit slits. The difference in spot size in horizontal and vertical direction is not visible with the reflective grating commonly used at ADRESS, as this analyzer does not provide horizontal resolution, and therefore, the horizontal size of the illumination spot has no effect on the spectral resolution. However, the horizontal spot size will be important for future 2D RIXS applications as described in the outlook.

5. Conclusion and outlook

We have demonstrated for the first time that diffractive transmission optics can be used as high-resolution RIXS analyzers providing stigmatic imaging properties. The resolving power achieved was E/dE = 6200 (incoming bandwidth E/dE_{BW} = 13000) in our first experiment, which is only about a factor two below the resolving power of E/dE = 13250 obtained with the reflective analyzer currently used at the ADRESS beamline and a smaller incoming bandwidth (E/dE_{BW} = 15000). This resolution is in good agreement with the theoretical predictions. The alignment of transmission FZP is very straight forward as they are very insensitive to alignment errors.

For further increasing the spectral resolution, the most promising step is to decrease the spot size of the illuminating beam on the sample, as this is the most limiting factor for the configuration used in our experiments. The increased fluence could lead to damage of radiation sensitive samples. However, the increase in fluence could be compensated by increasing the spot size in the non-dispersive direction. Additionally, as shown in Fig. 2, the

Optics EXPRESS

resolution can be increased by decreasing the period of the off-axis transmission FZP to enhance its dispersion. However, this would of course require improving the bandwidth of the incoming spectrum. Decreasing the effective line width could be possible for example by using a line doubling technique [22] or by designing the FZP to be used in a higher diffraction order.

Furthermore, diffractive transmission optics for soft x-rays with such small periods and high aspect ratios exhibit substantial volume effects, meaning that the grating cannot be treated as a two-dimensional element [23]. Tilting the optic by half of the diffraction angle α in respect to the incident beam can fulfil the Bragg condition, comparable to the situation in a multilayer mirror. This significantly increases the efficiency of such optics and can give values clearly exceeding those obtained with present RIXS spectrometer gratings.

Additionally, the number of detected scattered photons will be further increased by taking advantage of several simple considerations. For instance, the distance from sample to FZP can be reduced in future setups, resulting in a larger solid angle by the square of the distance reduction. Furthermore, the size of the optic can be increased as the flux of the signal scales linearly to its area. The longer electron beam writing time for larger area FZPs can be partially compensated by reducing the overhead time due to systematically following the rules for better fracturing of the layout [24]. Finally, a better efficiency of the FZP is possible by optimizing the fabrication process, an improvement by a factor of two seems to be realistic.

In our experiment, we demonstrated that the resolution of transmission off-axis FZPs is independent of the position of the sample, which enables advanced 2D RIXS schemes. For example, the RIXS sample can be illuminated by a line focus with varying incident energy on the long axis. Thus, a full set of RIXS spectra can be acquired in a single shot [14]. Using a homogeneous line focus for illumination, the investigated sample can be scanned acquiring a spatially resolved RIXS spectrum for each point of the scanned area. Thus, inhomogeneities and interfaces can be analyzed by their effect on the RIXS spectra.

The opportunity to record RIXS spectra in a spatially resolved manner generally opens a plethora of new experimental configurations, as a variety of parameters could be varied along the line focus. This includes thicknesses of deposited films, the strengths of external magnetic fields, temperature, or the impact of a pump laser. The latter option could be highly interesting in context RIXS measurements at XFEL sources when varying the arrival time of a pump laser with respect to the XFEL probe pulses along the line focus to obtain time-resolved RIXS spectra.

Funding

EU-H2020 Research and Innovation Programme, grant agreement No 654360 NFFA-Europe.

Acknowledgements

The authors are grateful to N. Opara for her assistance during sample preparation. Part of these experiments were performed at the Swiss Light Source, Paul Scherrer Institut,Villigen, Switzerland.